Food Packaging and Shelf Life 34 (2022) 100986

Contents lists available at ScienceDirect

Food Packaging and Shelf Life

journal homepage: www.elsevier.com/locate/fpsl

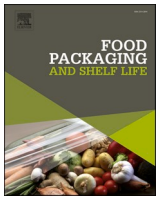

Central composite design optimization of active and physical properties of food packaging films based on chitosan/gelatin/pomegranate peel extract

Mirella Romanelli Vicente Bertolo [a], Lucas Danilo Dias [b], Josemar Gonçalves de Oliveira Filho [c,d], Fernanda Alves [b], Crisiane Aparecida Marangon [d], Virginia da Conceição Amaro Martins [a], Marcos David Ferreira [d], Vanderlei Salvador Bagnato [b,e], Ana Maria de Guzzi Plepis [a], Stanislau Bogusz Junior [a,*]

[a] University of São Paulo (USP), São Carlos Institute of Chemistry (IQSC), São Carlos, SP, Brazil
[b] University of São Paulo (USP), São Carlos Institute of Physics (IFSC), São Carlos, SP, Brazil
[c] São Paulo State University (UNESP), School of Pharmaceutical Sciences, Araraquara, SP, Brazil
[d] Brazilian Agricultural Research Corporation, Embrapa Instrumentação, São Carlos, SP, Brazil
[e] Texas A&M University – College Station Texas, Department of Biomedical Engineering, USA

ARTICLE INFO

Keywords:
Chitosan
Gelatin
Pomegranate peel extract
Packaging film
Multivariate optimization

ABSTRACT

Chitosan and gelatin-based materials containing pomegranate peel extract were prepared for potential application as food packaging materials. An optimized composition of 0.8% chitosan, 0.2% gelatin and 1 mg g^{-1} of extract was chosen with the aid of a central composite design, presenting low viscosity (8.36 ± 0.20 Pa s) and solubility (26.00 ± 5.50%), as well as an expressive inhibition halo against *Botrytis cinerea* (6.17 ± 0.36 mm). The interaction between the polymeric matrix and the extract was confirmed by spectroscopic and morphological analysis. Rheologically, the optimized formulation was more resistant to deformation and shear (activation energy increased by almost 5 kJ mol^{-1}) than the formulation without the extract. The use of pomegranate peel extract changed the film color, reduced its solubility (by more than 5%), increased mechanical resistance (tensile strength increased by 15 mPa), and improved light barrier properties by 30%. The extract also imparted antioxidant activity to the film, which was able to inhibit 20% of DPPH (2,2-diphenyl-1-picrylhydrazyl) radical at 38 mg mL^{-1}. The optimized composition also showed inhibitory bacterial properties (31.2 and 125 μg mL^{-1}) against *S. aureus* and *S. enteritidis*, respectively. Thus, the optimized film exhibited interesting characteristics for food packaging applications, many of them brought by the use of pomegranate peel extract, which highlights the valuable contribution of this agro-industrial waste to the properties of the polymeric films.

1. Introduction

The quality of food and food products during transportation, distribution, and storage can be affected by several factors, intrinsic and extrinsic to the food. The role of packaging is to protect the food, preventing its rapid deterioration and ensuring that a high-quality product reaches the consumer. Currently, the demand for natural and biodegradable materials has increased and several studies have focused on the development and characterization of biopolymeric films aiming their application in food packaging (Asdagh et al., 2021; Chen et al., 2022; Kumar, Petkoska, AL-Hilifi, & Fawole, 2021; Theapsak, Watthanaphanit, & Rujiravanit, 2012; Xue et al., 2021; Yuan, Yang, Chen & Sun, 2015).

Chitosan is a cationic polysaccharide with a linear chain, obtained from the partial deacetylation of chitin (Kurita, 2006). Its application in food preservation is increasing due to its nontoxicity, biodegradability,

Abbreviations: AAI, antioxidant activity index; BHI, Brain Heart Infusion; CCD, central composite design; CFU, colony forming units; CG, chitosan/gelatin film; CGPPE, chitosan/gelatin/pomegranate peel extract film; DPPH, 2,2-diphenyl-1-picrylhydrazyl; EB, elongation at break; FTIR-ATR, Fourier transform infrared spectroscopy with attenuated total reflectance; IC20, concentration necessary for 20% of inhibitory concentration; IC50, half maximal inhibitory concentration; LVR, linear viscoelastic region; MBC, minimal bactericidal concentration; MHB, Müeller Hinton broth; MIC, minimal inhibitory concentration; PPE, pomegranate peel extract; SEM, scanning electron microscopy; TPC, total phenolic content; TS, tensile strength; WCA, water contact angle; WVP, water vapor permeation.

* Correspondence to: Avenida do Trabalhador São Carlense, n° 400, São Carlos, SP, 13566-590, Brazil.
E-mail address: stanislau@iqsc.usp.br (S. Bogusz).

https://doi.org/10.1016/j.fpsl.2022.100986
Received 10 August 2022; Received in revised form 8 October 2022; Accepted 8 November 2022
2214-2894/© 2022 Elsevier Ltd. All rights reserved.

antimicrobial activity, and its ability to form films (Chen et al., 2022; Duan et al., 2019; Dutta, Tripathi, Mehrotra, & Dutta, 2009; Hu and Gänzle (2019); Konwar, Kalita, Kotoky and Chowdhury (2016); Yu, Yu, Zhao, Regenstein, & Xia, 2021; Yuan, Lv, Yang, Chen, & Sun, 2015). Combining chitosan with other polymers can improve the tensile properties and water-related effects of its films (Azaza et al., 2022). One of the most common polymers combined with chitosan for food applications is gelatin, a natural protein derived from collagen, that is also non-toxic, biodegradable, and safe for consumption (Ganeson et al., 2022; Poverenov et al., 2014). Such as chitosan, the study of gelatin-based films as protective packaging for food against light and gas exchange has also been extensively studied (Pirsa, Farshchi, & Roufegarinejad, 2020).

Although the combination of chitosan and gelatin has adequate properties that would guarantee a final material with good responses for food applications, its potential active properties deserve further investigation. The development of active polymeric films combined with plant extracts that can improve biological activity (i.e., antioxidant and antimicrobial) is at the forefront of food packaging research. Moreover, plant extracts are a sustainable alternative as they often come from agro-industrial waste, produced on a large scale (about 1 billion tons per year) by the agricultural industry. (Jabraili, Pirsa, Pirouzifard, & Amiri, 2021; Qin et al., 2015). Pomegranate (*Punica granatum* L.) peel is a food waste with elevated active potential, due to its phenolic compounds composition (Akhtar, Ismail, Fraternale, & Sestili, 2015; Bertolo, Martins, Plepis & Bogusz, 2021c). Several studies have described the combination of chitosan with pomegranate extracts for formulating packaging or edible films, always reporting improvements in the active properties of the films (Kumar et al., 2021; Pirsa, Sani, Pirouzifard, & Erfani, 2020; Yuan et al., 2015; Zeng, Ren, Zhu, & Gao, 2021; Bertolo, Martins, Horn, Brenelli, & Plepis, 2020; Bertolo, Leme, Martins, Plepis & Bogusz Junior, 2021a).

Another trend that is at the forefront of packaging development is the application of chemometric tools that shape the desirable characteristics of the material, while reducing the number of experiments, as well as the consumption of time, reagents and energy. The use of these mathematical and statistical tools makes it possible to predict the characteristics of materials, and how they may change according to the modification in the composition of the packaging (Istiqomah, Utami, Firdaus, Suryanti, & Kusumaningsih, 2022; Sharifi & Pirsa, 2021). Pirsa *et al.* (2020), evaluated, for example, the effect of percentages of gelatin and TiO2-Ag nanoparticles on the properties of carboxymethylcellulose-based films, using a central composite design. In this sense, the application of pomegranate peel extract (PPE) as an active component in chitosan and gelatin films and its influence on the optimization of the material composition, still unprecedented, can be studied.

Therefore, this study aimed to optimize the formulation composition of chitosan and gelatin-based films containing PPE with the aid of a central composite design (CCD), regarding their total phenolic content (TPC), viscosity, opacity, solubility, and water vapor permeability (WVP). To improve the optimization study and since chitosan has well-established antifungal activity, a zone of inhibition assay was also performed against two fungi of high incidence in foods (*Rhizopus stolonifer* and *Botrytis cinerea)* (Dutta et al., 2009). The optimized film composition was further characterized regarding its structural, rheological, physicochemical, optical, mechanical and active properties (antioxidant and antibacterial). These data will help propagate the use of multivariate optimization tools for the development of more efficient packaging and elucidate the impact of using pomegranate peel extract in polymeric films, bringing new insights into the valuable use of agro-industrial waste to improve the shelf life of foods.

2. Experimental section

2.1. Materials

Pomegranates (Peruvian variety) were washed, sanitized, and manually peeled. The peels were frozen and freeze-dried (Modulyo model, Edwards High Vacuum International, West Sussex, UK), crushed and stored at − 8 °C protected from light. The squid pens (*Doryteuthis* spp.) used to obtain chitosan were provided by Miami Comércio e Exportaç ão de Pescados LTDA (Cananéia, SP, Brazil). The gelatin used was type A, porcine, with ~300 Bloom (Sigma-Aldrich, St. Louis, Missouri, USA). All the solvents and reagents used in the following methodologies were PA grade or superior.

2.2. PPE and chitosan obtention

For PPE obtention, 15 g of pomegranate peel powder were extracted with an ethanolic solution 60% (v/v) (1:30, 45 °C, 1 h), in an ultrasonic bath (Unique USC-1400A, Indaiatuba, SP, Brazil) (Bertolo, Martins, Plepis, & Bogusz Junior, 2021b). After extraction and freeze-drying, the extract was stored protected from light at − 8 °C.

For chitosan obtention, β-chitin (extracted from squid pens) was submitted to a partial deacetylation process (NaOH 40%, 3 h, 80 °C, N_2 flow) (Horn, Martins, & Plepis, 2009). Chitosan obtained was of high molar mass (300 kDa), with 11.1% of acetylation degree (Rinaudo, 2006; Lavertu et al., 2003). The chitosan solution (1% w/w) was prepared in lactic acid (1% w/w), at room temperature for 24 h. The gelatin solution (1% w/w) was prepared in water (60 °C, 30 min) and gelled at 4 °C for 2 h.

2.3. Optimization of the film-forming solutions

To optimize the composition of the films regarding the amount of PPE (i.e., mg PPE g^{-1} solution) and chitosan (i.e., % chitosan), a CCD was conducted (Table S1). For each of prepared solutions, the percentage of gelatin was complementary to that of chitosan, keeping the final concentration of polymers at 1% in all solutions.

In total, 12 film-forming solutions were produced (Table 1). The solutions were prepared by adding the PPE ethanolic solutions (1 mL for each 50 g of mixture) into the 1% chitosan solution (w/w), under stirring for 2 h (500 rpm, 45 °C), followed by mixing the 1% gelatin solution (w/w). The solutions were weighed in Teflon® molds for the casting procedure. Five responses were evaluated in triplicate: TPC, viscosity, opacity, solubility, WVP and zone of inhibition test.

2.3.1. Characterization assays

2.3.1.1. Total phenolic content (TPC). The Folin-Ciocalteu method was used for TPC determination (Singleton, Orthofer, & Lamuela-Raventós, 1999). The solutions (50 mg mL^{-1}) reacted with Folin's reagent (2 N, Sigma-Aldrich) in 1:1 ratio for 5 min, sodium carbonate (20%, w/w, Dinâmica, Indaiatuba, SP, Brazil) was added to interrupt the reaction, and the absorbance was read after 15 min at 725 nm (Thermo Scientific™, Vantaa, Finland). Water was used as blank, and gallic acid (Sigma-Aldrich) as standard. TPC results were expressed in mg of gallic acid equivalent (GAE) mg^{-1} of film-forming solutions.

2.3.1.2. Viscosity. The viscosity was assessed with a shear rate between 0.1 and 1000 s^{-1}, at 25 °C, in an AR-1000 N controlled strain rheometer (TA Instruments, New Castle, DE, USA), with a stainless-steel plate cone geometry (20 mm diameter, 2° angle, and 69 μm gap) and a Peltier system for temperature control.

2.3.1.3. Thickness, solubility, and opacity. The thickness of the films was assessed at 20 random points with a micrometer M110–25 (Mitutoyo

Table 1
CCD matrix adopted to determine the proportions between the three film-forming solutions components, with the real and coded values of the variables adopted in each of the 12 experiments (A: mg PPE g^{-1} solution and B: % chitosan). Results of the analysis conducted with the 12 film-forming solutions (TPC, viscosity and zone of inhibition) and the 12 films (thickness, solubility, opacity, and WVP) from CCD.

N	A	mg PPE g^{-1}	B	% chitosan	TPC (mg GAE mg^{-1})	Viscosity (Pa s)	Thickness (mm)	Solubility (%)	Opacity (A mm^{-1})	WVP (g mm h^{-1} cm^{-2} Pa^{-1}(E-08))	Zone of inhibition (mm)	
											Rhizopus stolonifer	*Botrytis cinerea*
1	-1	1	-1	0.2	197.02 ± 7.01 $^{f, g}$	4.24 ± 0.61$^{d, e, f}$	0.034 ± 0.004^{e}	19.80 ± 3.54$^{b, c}$	10.49 ± 1.12$^{c, d}$	1.97 ± 0.15^{d}	–	–
2	1	3	-1	0.2	531.75 ± 21.58^{a}	1.59 ± 0.27 ^{g}	0.041 ± 0.002$^{b, c}$	28.62 ± 5.44$^{a, b, c}$	15.06 ± 1.12$^{a, b}$	2.22 ± 0.08^{d}	–	–
3	-1	1	1	0.8	169.65 ± 16.79 ^{g}	8.36 ± 0.20^{c}	0.035 ± 0.004$^{d, e}$	26.00 ± 5.50$^{a, b, c}$	12.01 ± 0.29^{c}	2.75 ± 0.02$^{a, b, c}$	–	6.17 ± 0.36^{b}
4	1	3	1	0.8	246.49 ± 28.05 ^{f}	5.40 ± 0.16^{d}	0.040 ± 0.005$^{c, d}$	27.77 ± 0.49$^{a, b, c}$	16.96 ± 0.83^{a}	3.54 ± 0.05^{a}	6.49 ± 0.42^{b}	9.78 ± 1.33$^{a, b}$
5	0	2	0	0.5	312.81 ± 4.25^{e}	2.33 ± 0.07 $^{f, g}$	0.043 ± 0.003$^{b, c}$	23.78 ± 0.64$^{b, c}$	14.50 ± 0.98^{b}	2.69 ± 0.03$^{b, c, d}$	–	–
6	0	2	0	0.5	359.47 ± 19.56$^{c, d, e}$	2.48 ± 0.19$^{e, f, g}$	0.043 ± 0.004$^{b, c}$	23.35 ± 1.37$^{b, c}$	15.30 ± 0.58$^{a, b}$	2.77 ± 0.05$^{a, b, c}$	–	–
7	0	2	0	0.5	331.05 ± 34.80$^{d, e}$	2.70 ± 0.19$^{e, f, g}$	0.043 ± 0.003$^{b, c}$	22.13 ± 0.31^{c}	14.36 ± 0.36^{b}	2.77 ± 0.11$^{a, b, c}$	–	–
8	0	2	0	0.5	315.96 ± 7.01^{e}	2.31 ± 0.12 $^{f, g}$	0.043 ± 0.003$^{b, c}$	22.77 ± 4.74^{c}	14.32 ± 0.69^{b}	2.74 ± 0.03$^{a, b, c, d}$	–	–
9	-1.41	0.59	0	0.5	100.53 ± 7.37 ^{h}	4.51 ± 0.14$^{d, e}$	0.046 ± 0.004^{b}	29.50 ± 0.66$^{a, b, c}$	10.37 ± 0.40$^{c, d}$	2.54 ± 0.02$^{c, d}$	–	–
10	1.41	3.41	0	0.5	465.44 ± 8.83^{b}	2.29 ± 0.07 $^{f, g}$	0.052 ± 0.005^{a}	29.84 ± 0.20$^{a, b, c}$	14.79 ± 0.69^{b}	2.44 ± 0.09$^{c, d}$	–	–
11	0	2	-1.41	0.08	388.25 ± 17.31^{c}	17.01 ± 2.32^{a}	0.042 ± 0.005$^{b, c}$	50.74 ± 3.90^{a}	8.55 ± 0.30^{d}	2.40 ± 1.15$^{c, d}$	–	–
12	0	2	1.41	0.92	345.43 ± 21.37$^{c, d, e}$	11.31 ± 0.10^{b}	0.056 ± 0.005^{a}	31.98 ± 1.17$^{a, b}$	10.58 ± 0.26$^{c, d}$	3.07 ± 0.13$^{a, b}$	16.63 ± 2.60^{a}	13.13 ± 1.73^{a}

In the same column, values with different superscript letters indicate statistically significant differences by ANOVA and Tukey ($p \leq 0.05$).

Mfg. Co., Kanagawa, Japan), after stabilization at a relative humidity (RH) of 75%.

Solubility (Eq. (1)) was determined according to Peng, Wu, and Li (2013): after weighing the initial dry film (W_1), the films were placed in deionized water (10 mL) and shaken for 6 h at 25 °C. After drying (80 °C for 24 h), the weight of the final dry film (W_2) was determined.

$$Solubility \quad (\%) = \left(\frac{W_1 - W_2}{W_1}\right) x \quad 100 \tag{1}$$

The opacity of the films (Eq. (2)) was determined by the ratio between their absorbance at 600 nm (U-300 spectrophotometer, HITACHI, Tokyo, Japan) and their thickness (L, in mm) (Peng & Li, 2014).

$$Opacity \quad \left(A \quad mm^{-1}\right) = \frac{Abs_{600 \quad nm}}{L} \tag{2}$$

2.3.1.4. Water vapor permeability (WVP). For WVP determination (Eq. (3)), permeation cups containing 6 mL of deionized water were sealed with the films, weighed and put in an air circulation oven (SL-102, Solab, Piracicaba, SP, Brazil) at 40 °C and RH = 0%. The weight of the cups was determined every 2 h for 10 h and at 32 h (ASTM E96/E96M-16 (ASTM, 2016; Oliveira Filho et al., 2020).

$WVP(\text{g mm h}^{-1}\ \text{cm}^{-2}\ \text{Pa}^{-1}) = \frac{m}{t\ A\Delta p}$ Eq. (3).

In the equation, m is the mass loss of the cups containing the films, A is the area of the film sealed in the cup, t is the analysis time and Δp is the difference in the water vapor pressure in the cups.

2.3.1.5. Antifungal activity. The in vitro antifungal activity of the film-forming solutions was evaluated against *Rhizopus stolonifer* and *Botrytis cinerea,* two fungi of high incidence in foods, by the zone of inhibition assay. Briefly, 200 μL of fungal spore solutions (10^5 spores mL^{-1}) were inoculated onto plates with Potato Dextrose Agar (PDA, Kasvi, São José do Pinhais, PR, Brazil). Perforations of 10 mm in diameter were made on the agar and 50 μL of the solutions were placed in the perforations. The diameters of the zones of inhibition were measured after incubation (37 °C) for 48 and 168 h for each fungus, respectively (Oliveira Filho et al., 2019).

The antibacterial activity of the final optimized composition was also evaluated later, as described in Section 2.4.4.

2.4. Characterization of the optimized film composition

The best composition of the film-forming solution (CGPPE) was characterized regarding structural, rheological, physicochemical, optical, and tensile properties. The optimized film was also evaluated regarding its active properties (antioxidant and antibacterial activity). A chitosan and gelatin (CG) sample (without PPE) was prepared and analyzed as a control experiment.

2.4.1. Spectroscopic and morphological analysis

The Fourier-transform infrared spectra with attenuated total reflectance (FTIR-ATR) of PPE, CG, and CGPPE were obtained with 2 cm^{-1} resolution and 16 scans, from 4000 to 650 cm^{-1} (FT-IR spectrometer - Cary 630, Agilent Technologies, Santa Clara, CA, USA). Their fluorescence emission spectra were obtained from 380 to 700 nm, after excitation of the samples at 370 nm (Cary Eclipse Fluorescence spectrophotometer, Agilent Technologies). Raman spectra of CG and CGPPE were obtained on a WITec Alpha 300 RAS microscope (WITec, Ulm, Germany), by excitation in 785 nm and detection from 0 to 3500 cm^{-1}. A 20-x magnification objective (Zeiss, Jena, Germany) collected the spectra.

For scanning electron microscopy (SEM), CG and CGPPE were covered with a gold layer (6 mm thickness, Coating System MED 020 metallizer, BAL-TEC, Liechtenstein). To obtain cross-sectional surface images, the films were fractured and fixed onto 90° specimen stubs. The microscope was a ZEISS LEO 440 (Cambridge, England), with a model 7060 OXFORD detector and 20 kV electron beam.

2.4.2. Rheological properties

A rheological study of CG and CGPPE film-forming solutions was conducted using an AR-1000 N controlled strain rheometer. Strain sweep measurements were determined from 0.05 to 500 Pa at 25 °C and 1.0 Hz. G' and G'' moduli were determined by varying the angular frequency (0.1–100 rad s^{-1}, 25 °C, 10% of strain), and temperature (25–75 °C, 5 °C min^{-1}, 1.0 Hz, 10% of strain). Finally, flow measurements were conducted, varying the shear stress (0.5–1000 s^{-1}) at different temperatures (Bertolo, Leme, Martins, Plepis, & Bogusz Junior, 2021a).

2.4.3. Physicochemical, optical, and tensile properties

The moisture content of CG and CGPPE was determined by the difference in weighing before and after their stabilization at 15% RH for 7 days. Their swelling (Eq. (4)) was determined by immersing the films (W_1) in 10 mL of deionized water and weighing (W_2) at specific time intervals (30 min, 1, 2, 4 and 6 h) (Peng et al., 2013). Likewise, their solubility was evaluated as a function of time, as described in Section 2.3.1.3.

$$Swelling \quad (\%) = \left(\frac{W_2 - W_1}{W_1}\right) x100 \tag{4}$$

The hydrophilicity of CG and CGPPE was determined by contact angle measurements (CAM200 goniometer, KSV Instruments, Finland). Water droplets (5 μL) were placed on the surface of the film. The contact angle was taken in 10 frames every 1 s and calculated with the CAM 2008 software (Young/Laplace adjustment method).

The optical properties of the films (lightness/darkness (L*), chroma (C*), hue angle (h°), and total color difference (ΔE*)) were obtained with a HunterLab colorimeter (HunterLab, Reston, USA, CIELab system). Optical barrier properties were evaluated from 250 to 800 nm (Shimadzu 1600, Portland, USA). Finally, tensile tests were conducted in a Texture Analyzer TA. XT Plus equipment (Stable Micro Systems, Surrey, UK), following the D882–12 method (ASTM, 2012).

2.4.4. Active properties

2.4.4.1. Total phenolic content and DPPH radical inhibition. The antioxidant activity of PPE, CG, and CGPPE against DPPH radical (Sigma-Aldrich) was determined by reacting a 0.1 mmol L^{-1} radical solution with ethanolic PPE solutions (3.125–100 μg mL^{-1}) (Pal, Raju, Pandey, Raj, & Singh, 2017). CG and CGPPE (20–80 mg mL^{-1}) were also placed to react with the radical. Absorbance decay was monitored at 517 nm for 30 min (Thermo Scientific™ model Multiskan GO), and % inhibition was calculated (Eq. (5)). IC_{50} was determined using a curve of a percentage of inhibition versus the log of PPE concentration (Chen, Bertin, & Froldi, 2013). The AAI (antioxidant activity index) of the samples was calculated according to Eq. (6) (Scherer & Godoy, 2009). The TPC of PPE, CG and CGPPE was determined as described in Section 2.3.1.1.

$$DPPH \quad inhibition \quad (\%) = \left(\frac{Abs_{DPPH} - Abs_{sample}}{Abs_{DPPH}}\right) x \quad 100 \tag{5}$$

$$AAI = \left(\frac{DPPH \quad concentration}{IC_{50}}\right) x \quad 100 \tag{6}$$

2.4.4.2. Minimum inhibitory concentration (MIC) and minimum bactericidal concentration (MBC). MIC and MBC of PPE, CG, and CGPPE solutions against bacterial strains (*Staphylococcus aureus* ATCC 25923 and *Salmonella enterica* Enteritidis ATCC 13076) were carried out with the broth microdilution assay Clinical and Laboratory Standards Institute (2018). The samples were serially diluted with Müeller-Hinton broth (MHB, pH 5.5, Himedia, Mumbai, India), with initial concentrations of 2000 μg mL^{-1} for PPE and 500 μg mL^{-1} for CG and CGPPE (pH 5.0). The overnight cultures were diluted to a final population of 5×10^5 colony-forming units (CFU) mL^{-1} per well. The optical density at 600 nm was measured after 18 h at 37 °C (Perkin Elmer EnSpire, Waltham, Massachusetts, USA). Wells with no visible growth were placed in MHB agar plates and incubated for 24 h for MBC determination. MIC was identified as the lowest sample concentration in which no apparent growth was detected, and MBC was the lowest sample concentration without viable cells.

2.5. Statistical analysis

The software Statistica® v. 13 (Statsoft Inc., Tulsa, OK, USA) was used for CCD analysis, to choose the best film composition and to build the Pareto diagrams. The software Action® (Estatcamp Team, São Carlos, SP, Brazil) was used for the ANOVA and Tukey tests conducted in the CCD analysis and in the optimized film analysis.

3. Results and discussion

3.1. Optimization of the film-forming solutions

Table 1 shows the results of the analysis carried out with the 12 samples of CCD. To choose the best formulation of the film-forming solutions, their TPC should be of considerable value (demonstrating their antioxidant potential), while their viscosity should be low, since high viscosity materials have numerous experimental challenges (Bertolo et al., 2021a; Nair, Jyothi, Sajeev, & Misra, 2011). The responses of solubility and WVP were pursued to be minimized, since it is not desirable for the films to disintegrate in contact with water and to allow the excessive passage of water vapor. Besides, the films must act as potential barriers to the passage of light, which means that their opacity needs to be maximized. The in vitro antifungal activity results were also considered to choose the best formulation, even though only some experimental assays showed significant results in CCD (Table 1). Thickness, also shown in Table 1, was not included as a response in CCD, but it was necessary to calculate the opacity and WVP of the films.

Fig. 1 shows the response surface graphs obtained by the interaction between the variables % of chitosan and PPE concentration, for each of the 5 responses evaluate. In general, both variables had a significant influence (Pareto diagrams for all responses are found in Fig. S1) on the analysis: PPE concentration showed highly significant effects for the TPC, since the phenolics in the extract are the ones responsible for the phenolic content of the solutions. In addition, increasing the amount of PPE led to films with a greater opacity, which also reflected in a significant and high effect of this variable for that response.

For the other responses, % of chitosan was the variable of highest significant influence with positive effects, which means that higher concentrations of this polymer maximized the viscosity, as well as the solubility and WVP of the films. Therefore, the physicochemical results of CCD indicated that moderate concentrations of chitosan would be more adequate for a balance between the desired responses (lower viscosity, solubility, and WVP).

However, the results of in vitro antifungal activity of the film-forming solutions against *Rhizopus stolonifer* and *Botrytis cinerea* revealed that higher concentrations of chitosan were needed to ensure antifungal effect: only formulations 4 and 12 showed a zone of inhibition against both fungi, and for *Botrytis cinerea* the inhibition was also detected in solution 3 (Table 1). The common variable between these three samples was the high chitosan concentration. The diameters of the zones of inhibition increased with the increase of the percentage of chitosan in the solution, for the same fungus. Additionally, an increase in three times in the amount of PPE, from 1 mg g^{-1} to 3 mg g^{-1}, increased the zone of inhibition against *Botrytis cinerea* from 6.17 ± 0.36 mm to 9.78 ± 1.33 mm, which suggests that the presence of the extract may have contributed to antifungal activity.

Aiming to minimize the viscosity, WVP, and solubility of the films, but also to keep the antifungal activity of the film-forming solutions, sample 3 was chosen as the best film composition. Film 3 showed lower

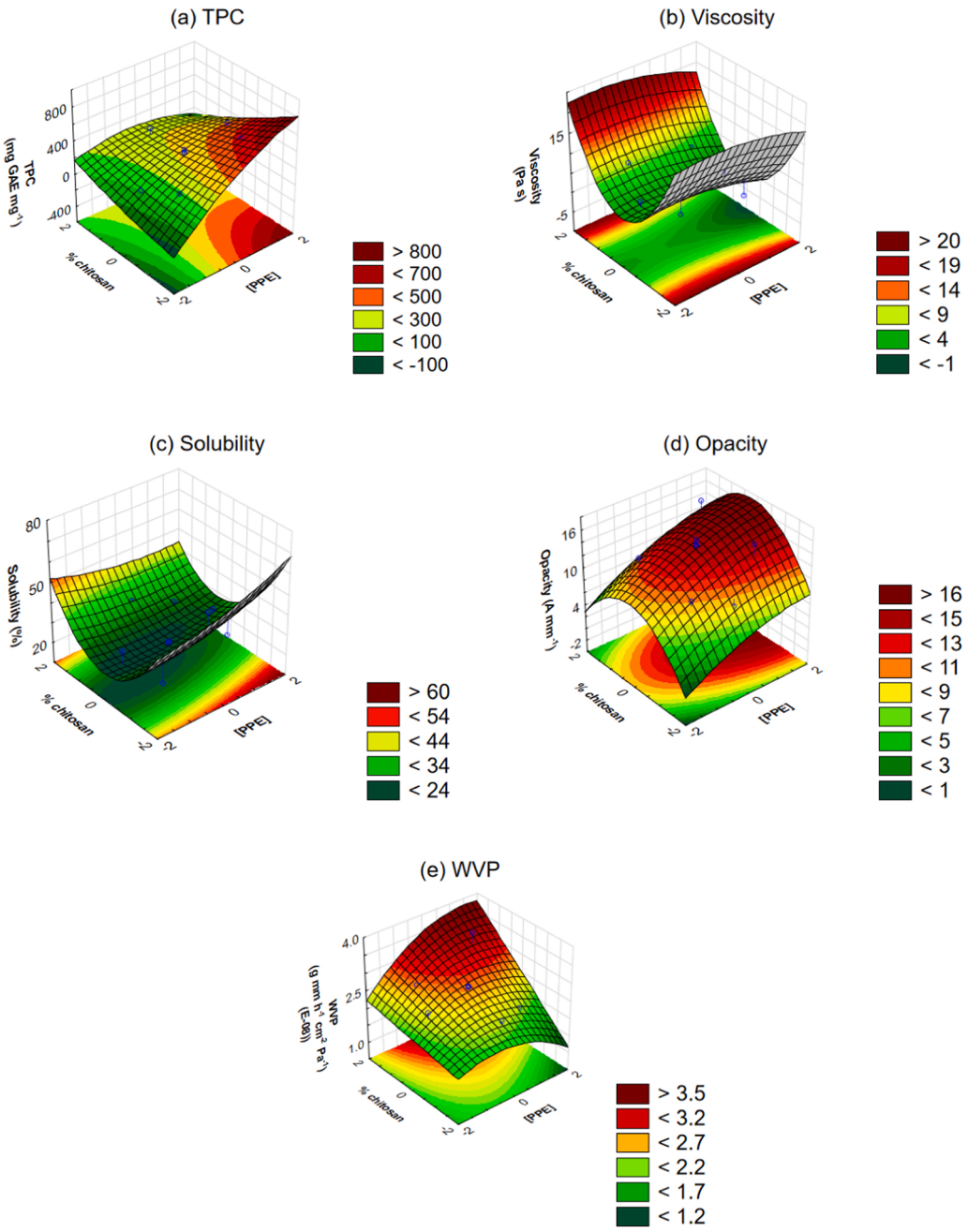

Fig. 1. Response surface plots obtained by the interaction between the two variables (% chitosan × [PPE]) for the film-forming solutions from CCD, regarding their: (a) TPC, (b) viscosity, (c) solubility, (d) opacity, and (e) WVP.

solubility and WVP than samples 4 and 12, and the viscosity of its forming solution was lower than that of solution 12. Furthermore, despite the lower TPC, solution 3 was able to inhibit *Botrytis cinerea* in the in vitro model, suggesting promising results for the intended application, since the concentrations of microorganisms present in food tend to be much lower than those tested in the zone of inhibition assay.

3.2. Characterization of the optimized film composition

3.2.1. Spectroscopic and morphological analysis

The spectroscopic analysis described below were carried out to characterize the materials and to observe the interaction between the phenolic compounds of the extract and the polymeric matrix in CGPPE, compared to the optimized composition without extract (CG). Fig. 2(a) shows the FTIR-ATR spectra obtained for PPE: at 3273 cm^{-1}, there is broadband related to the stretching of the O-H bonds of the alcohol, phenol, and carboxylic groups present in the phenolic compounds (Ay, Özcan, Erdoğan, & Özcan, 2012). The slight band at 2922 cm^{-1} refers to the C-H stretching of methyl, methoxyl, and methylene groups present in phenolic acids. The neighboring bands in 1715 and 1602 cm^{-1} represent the C═O bonds found in carbonyls and the C═C bonds of aromatic rings, respectively (Edison & Sethuraman, 2013). At 1341, 1200 and 1028 cm^{-1}, the bands can be attributed to the stretching of N-H bonds in secondary amines, C-H in aromatics, and C-C-N in amines (Bertolo et al., 2020; Salem, Albanna, & Awwad, 2017).

Regarding CG and CGPPE, a subtle difference is found in the region of 3350 cm^{-1}, characteristic of the stretching of the N-H bonds from the amino groups of chitosan and the amide A of gelatin. For CGPPE, a slight broadening of the band in this region was observed, due to the stretching of the O-H bonds of the PPE phenolic compounds, a first indicative of the

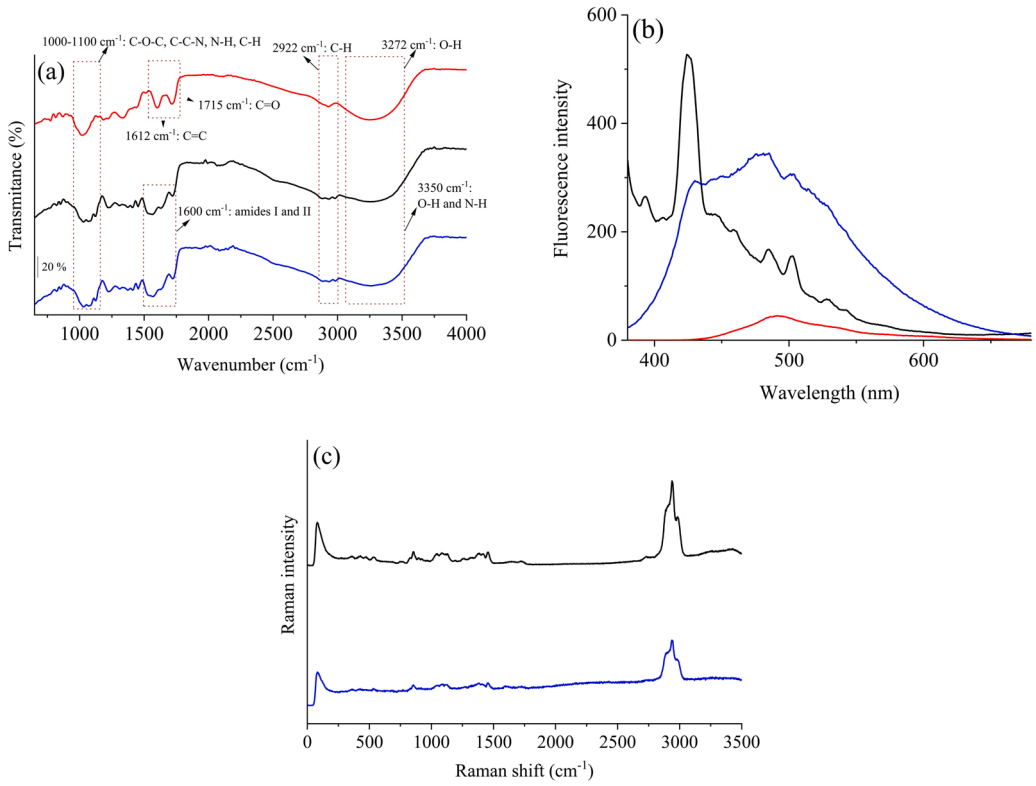

Fig. 2. (a) FTIR-ATR spectra for: (——) PPE, (—) CG, and (——) CGPPE; (b) Fluorescence spectra after excitation at 370 nm for (——) PPE, (—) CG, and (——) CGPPE; (c) Raman spectra for (—) CG and (——) CGPPE.

incorporation of the extract to the polymeric matrix. The bands representing amides I and II of chitosan and amide I of gelatin appear around 1600 cm^{-1}; the three near bands between 1000 and 1100 cm^{-1} refer to the C-O-C bonds of chitosan, as well as the N-H, C-H and C-C-N bonds of PPE and the polymers (Xu *et al.* 2006).

Fig. 2(b) shows the fluorescence spectra of PPE, CG, and CGPPE after excitation at 370 nm: PPE showed a broader peak with a lower intensity, with its maximum around 480 nm. For CG, an intense emission peak was observed around 425 nm, which is attributed by the literature as resonance fluorescence (Mi, 2005). With the incorporation of PPE to CGPPE,

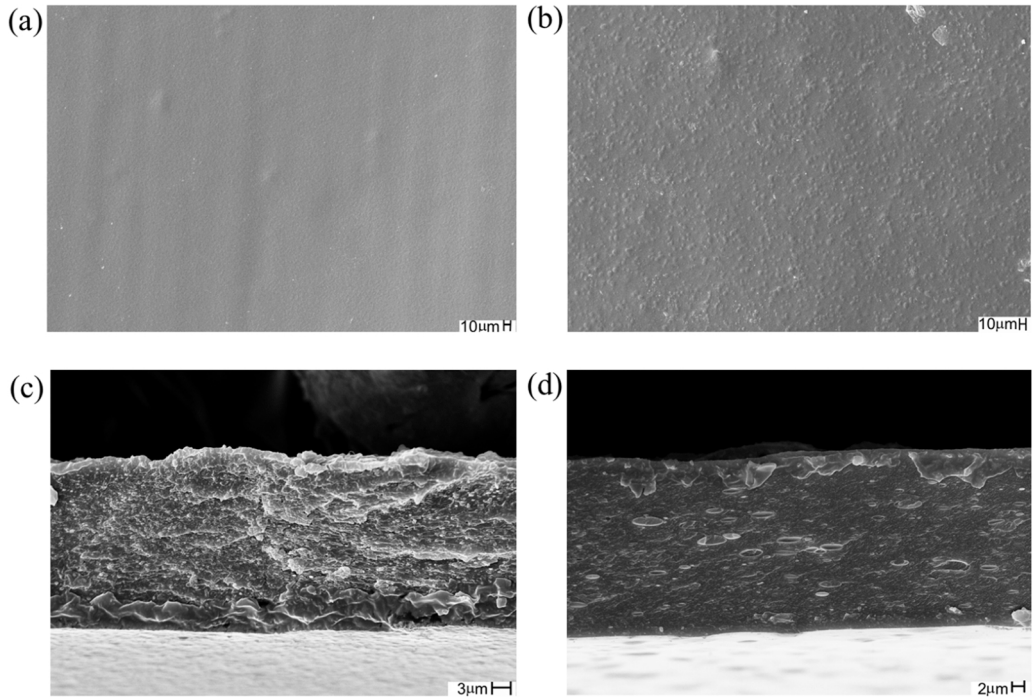

Fig. 3. SEM surfaces of (a) CG and (b) CGPPE, both at 500 × magnification; SEM cross-sectional surfaces of (c) CG and (d) CGPPE, both at 5000 × magnification.

however, the well-defined and intense peak changed to a broader region with lower intensity around 480 nm, coinciding with the maximum observed for PPE. This demonstrates that the energy of the excited state of PPE was changed with its inclusion in the polymeric matrix, probably due to the new interactions between the phenolic groups from the extract with the amino and carboxylic groups of the polymers.

The Raman spectra of CG and CGPPE films (Fig. 2(c)) showed a peak of maximum intensity located around 2940 cm^{-1}, typical of polymers (C-H vibrations). For CGPPE, the maximum Raman intensity reached by this peak was about 17% lower than in CG. CG also presented peaks of greater intensity and better defined than in CGPPE, in the regions of 860 (C-C vibrations), 1080 (C-N and C-O-C bonds vibrations) and 1455 cm^{-1} (CH_2 scissoring, C-H and O-H bonds) (Eddya, Tbib, & Hami, 2020; Frushour & Koenig, 1975). Once again, the spectroscopic results indicate the interaction formed between PPE and the polymers, which explains the lower intensities found for chitosan and gelatin typical assignments in CGPPE Raman spectra.

Fig. 3 shows the surface (a and b) and cross-sectional surfaces (c and d) SEM images of CG and CGPPE films: CG presented a smooth surface, without precipitates. The addition of PPE to CGPPE led to a different surface morphology, with the visible presence of the extract distributed over the entire surface. The compact and brittle structure observed for CG changed to a less compact cross-sectional surface with extract agglomerates. The structural differences observed for CG and CGPPE films can significantly impact film characteristics, such as their water-related properties (since the extract and its hydrophilic nature conflict with the predominantly hydrophobic nature of chitosan, which explains the aggregates in the cross-sectional images), as well as their rheological and

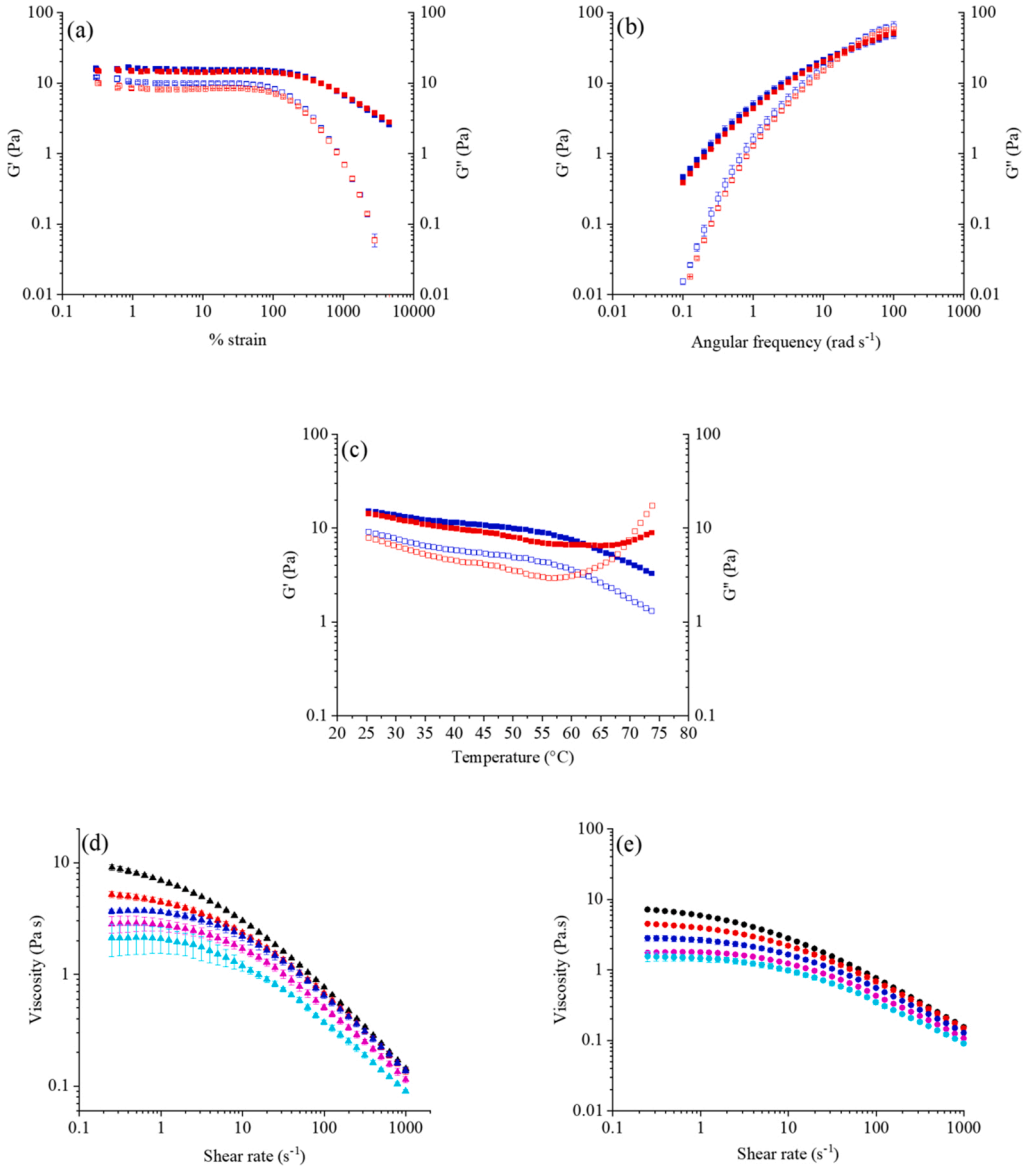

Fig. 4. G' and G'' moduli for CG (■) and CGPPE (■) related to (a) % strain, (b) angular frequency, and (c) temperature. Viscosity as a function of shear rate at different temperatures for (d) CG (▲ 15 °C, ▲ 25 °C, ▲ 35 °C, ▲ 45 °C, and ▲ 55 °C) and (e) CGPPE (● 15 °C, ● 25 °C, ● 35 °C, ● 45 °C, and ● 55 °C).

mechanical properties.

3.2.2. Rheological properties

To better understand the interactions formed between PPE and the polymers in the film-forming solutions, a complete rheological study was carried out with CG and CGPPE. Fig. 4(a) shows the mean strain curves obtained: in both cases, G'' > G', indicating the predominance of the viscous (G'') modulus over the elastic (G') one. From these curves, γ_L was determined (Table 2), the highest percentage of deformation to which the solutions can be submitted before leaving the linear viscoelastic region (LVR) (region where G' and G'' are constant) (Fadavi, Mohammadifar, Zargarran, Mortazavian, & Komeili, 2014). The higher γ_L, the greater the structural strength of the solution. PPE inclusion in CGPPE led to a tendency of increasing γ_L, indicating that the extract may be reinforcing the polymeric structure.

PPE significantly decreased G'_{LVR} (G' value at LVR limit) in CGPPE, which can also be perceived by the increase in tanδ (G''/G') values (Table 2). tanδ classify the samples in oscillatory rheological assays: if tanδ > 1, the samples can be classified as viscous, as is the case of CG and CGPPE; if tanδ > 0.1, the sample is in an intermediate state between a real gel and a concentrated polymeric solution, which also applies to the film-forming solutions of this study (Mandala, Savvas, & Kostaropoulos, 2004).

Fig. 4(b) shows G' and G'' moduli against the applied angular frequency: for both solutions, G'' > G' in most of the applied frequency range; however, a crossover was observed, and at the end the elastic modulus prevailed in both cases, a behavior typical of concentrated polymeric solutions (Naji-Tabasi, Mohammad, & Razavi, 2017; Steffe, 1996). The $\omega_{crossover}$ and $G'_{crossover}$ values (Table 2) indicate that PPE incorporation significantly delayed ($p \leq 0.05$) the inversion between the moduli by about 4 rad s^{-1}. These results agree with those of the strain sweep measurements, as they suggest that PPE may be forming new interactions with the polymeric mixture, reinforcing its resistance to change in the face of deformation and frequency applied.

Fig. 4(c) shows how the moduli vary with the temperature: up to approximately 55 °C, both G'' and G' moduli decreased with the temperature increment, a behavior typical of polymers. However, for CGPPE the moduli started to rise around 60 °C, crossing at 63.80 ± 4.81 °C. This crossover can be explained by the reduction of hydrogen interactions existing between the polymeric network and the water molecules, which at high temperatures are energized and eliminated from the mixture. Thus, the polymer-polymer interaction is reinforced, leading to an increase in the elasticity of the solution, and to the consequent crossover of the moduli (Tang, Guan, Yao, & Zhu, 2007). As the presence of PPE had already decreased the interactions of the polymers with water, such crossover due to increased temperature was facilitated in CGPPE.

The impacts of shear rate on the viscosity were also evaluated with temperatures ranging from 15° to 55°C (Fig. 4d and e), and the Cross model was used to model the curves (Eq. (7)). In the equation, η_0 and η_∞ are the viscosities at zero shear and maximum at infinite shear (both in Pa s), γ is the shear rate (s^{-1}), k is the consistency index (s), and n is the rate index (dimensionless).

$$\frac{\eta - \eta_\infty}{\eta_0 - \eta_\infty} = \frac{1}{(1 + (k\gamma)^n)} \quad (7)$$

CG and CGPPE showed a pseudoplastic behavior, since a reduction in their viscosity was observed with an increase in the shear rate for all temperatures studied (Mandala et al., 2004). η_0, which represents the viscosity of the materials when the polymer molecules are still randomly distributed, tended to decrease with increasing temperature for both solutions (Table 2). Finally, the viscosity of the solutions was related to the temperature with the Arrhenius equation (Eq. (8)), where E_a is the activation energy, R is the Gas Constant (8.3144 J K^{-1} mol^{-1}), and A is a constant.

$$\ln \eta_0 = \ln A - (E_a/R) \times (1/T) \quad (8)$$

Activation energy is the energy necessary for the molecules of a fluid to move, causing it to flow. The higher E_a, the greater is the resistance of the fluid to flow, due to stronger molecular interactions (Abbastabar, Azizi, Adnani, & Abbasi, 2015). E_a significantly increased from CG to CGPPE (Table 2), another result that suggests that the incorporation of PPE made the polymeric network more resistant to the applied shear.

Table 2
Rheological features of CG and CGPPE, obtained by strain, angular frequency, temperature, and flow measurements: critical strain (γ_L), G' modulus at the LVR limit (G'LVR), loss tangent value (tanδ), angular frequency and G' modulus at the moduli crossover ($\omega_{crossover}$ and $G'_{crossover}$), initial viscosity (η_0) according to the temperature, as well as the energy of activation (E_a) for CG and CGPPE. Physicochemical, optical, and tensile properties of CG and CGPPE films.

Rheological parameters	CG	CGPPE
γ_L (%)	65.67 ± 2.76[a]	68.47 ± 1.33[a]
G'_{LVR} (Pa)	9.30 ± 0.56[a]	7.94 ± 0.14[b]
tanδ	1.63 ± 0.02[b]	1.80 ± 0.02[a]
$\omega_{crossover}$ (rad s^{-1})	19.49 ± 1.05[b]	23.74 ± 0.82[a]
$G'_{crossover}$ (Pa)	27.78 ± 2.47[a]	29.87 ± 0.55[a]
η_0 (Pa s)		
15 °C	10.10 ± 0.53[a]	8.05 ± 0.30[b]
25 °C	5.58 ± 0.37[a]	4.87 ± 0.11[b]
35 °C	3.91 ± 0.18[a]	3.00 ± 0.29[b]
45 °C	3.01 ± 0.47[a]	1.86 ± 0.03[b]
55 °C	2.34 ± 0.86[a]	1.62 ± 0.21[a]
E_a (kJ mol^{-1})	28.01 ± 2.57[a]	32.91 ± 2.62[a]
Films parameters	**CG**	**CGPPE**
Thickness (μm)	30 ± 8[a]	35 ± 7[a]
Moisture content (%)	8.01 ± 1.54[a]	9.28 ± 2.06[a]
Solubility (%) * *	28.45 ± 7.33[a]	23.15 ± 1.63[a]
Swelling (%) * *	4453 ± 1490[a]	350.64 ± 28.12[b]
WCA (°)	109.76 ± 6.36[a]	89.24 ± 2.01[b]
L*	92.34 ± 0.31[a]	88.46 ± 0.16[b]
h°	125.00 ± 2.72[a]	94.90 ± 0.32[b]
C*	1.98 ± 0.15[b]	19.51 ± 0.46[a]
ΔE*	6.57 ± 0.31[b]	21.65 ± 0.38[a]
TS (mPa)	30.00 ± 0.69[b]	45.31 ± 1.08[a]
EB (%)	4.28 ± 0.77[b]	9.07 ± 2.01[a]

Different lowercase letters on the same line show statistically significant differences by ANOVA and Tukey ($p \leq 0.05$). * * Values after 6 h of immersion in water.

3.2.3. Physicochemical, optical, and tensile properties

Table 2 also shows the physicochemical properties of CG and CGPPE films, thickness, moisture content, and solubility were not significantly ($p > 0.05$) affected by PPE incorporation. Nevertheless, a tendency of increasing film thickness was observed in CGPPE, as well as an increase in its moisture, and a decrease in its solubility. The solubility and swelling of the films were also evaluated as a function of time (Fig. S2). CGPPE showed stable solubility over time, never exceeding 25%. CG, in turn, presented values up to 35%, mainly due to the rapid swelling of the films, which lost their defined structure. Both CG and CGPPE presented a rapid swelling, stabilized after 30 min, but CG swelled about 13 x more than CGPPE (Table 2).

Therefore, PPE incorporation was able to decrease both the solubility and the swelling of the chitosan/gelatin films, which are two of the main water-related properties to be minimized when considering their application as packaging. The increment in the number of intermolecular interactions between the phenolic compounds of PPE and the polymers (which were already confirmed by the spectroscopic and rheological analysis) may have decreased the affinity of chitosan and gelatin chains with water, thus improving the water-related properties of the films. Kaya et al. (2018) reported similar results for the solubility of chitosan films with the addition of *Berberis crataegina* extract. PPE also led to a significant decrease in the water contact angle (WCA) on the surface of CGPPE, decreasing the hydrophobicity of the film (Table 2).

Such a result is related to an increase in the wettability since the extract presents a hydrophilic nature. This effect can also be seen in Fig. S3, which shows the profile of the water drop on the surface of CG and CGPPE films. Despite the decrease in the mean value of WCA in CGPPE, however, its surface remained predominantly hydrophobic (WCA ~ 90°).

Not only the water-related properties are important to be evaluated when it comes to films for food packaging, but also their optical properties: PPE addition significantly decreased the L* (lightness/darkness) parameter, indicating that the extract led to darker chitosan/gelatin-based films. Yuan et al. (2015) also observed a decrease in the lightness of chitosan films with carvacrol and pomegranate peel extract. The hue angle (h°) also decreased significantly with PPE incorporation, changing the color of the films from the green (180°) to the yellow (90°) region (Oliveira-Filho et al., 2020). The chroma (C*) and the total color difference (ΔE*), in turn, significantly increased from CG to CGPPE.

The percentage of light transmittance of the films in the UV and visible regions was evaluated (Fig. 5). The lower the transmittance, the better the ability of the film to protect the packaged food from light-induced oxidative processes (Oliveira-Filho et al., 2020). PPE addition reduced about 30% the transmittance of chitosan/gelatin films, at 400 nm. Even in the visible region, the percentages of transmittance found for CGPPE were lower than for CG, stabilizing around 50%. Thus, PPE also improved the barrier properties of the films against the passage of visible and ultraviolet light, due to the unsaturated bonds present in its components that are capable of absorbing UV-Vis radiation (C═O, C═N, and C═C) (Hu, Yao, Qin, Yong, & Liu, 2020). Such effect had already been predicted by the opacity test in CCD, which indicated a positive relationship between the amount of extract and the light barrier property of the films.

Finally, the tensile properties of CG and CGPPE films are also presented in Table 2; PPE significantly increased the tensile strength (TS) and the elongation at break (EB) of the films. Similar results have been reported for chitosan/gelatin films incorporated with quercetin, rutin, and cinnamon essential oil, all intended to be used as packaging active components (Roy & Rhim, 2021, Narasagoudr et al., 2020). The enhanced tensile properties can be explained by the solid interfacial interactions (like H-bonds) between the phenolics from PPE and the polymeric matrix, as also suggested by the previous results: the greater the interactions between the components of the film, the higher the strength necessary to promote its rupture.

3.2.4. Active properties

The TPC of PPE, CG and CGPPE are shown in Table 3. TPC of CGPPE corresponds to 89.6% of the PPE added into it, which portrays the successful incorporation of the extract into the material. The IC_{50} against DPPH radical found for PPE by the sigmoidal adjustment of its curve of

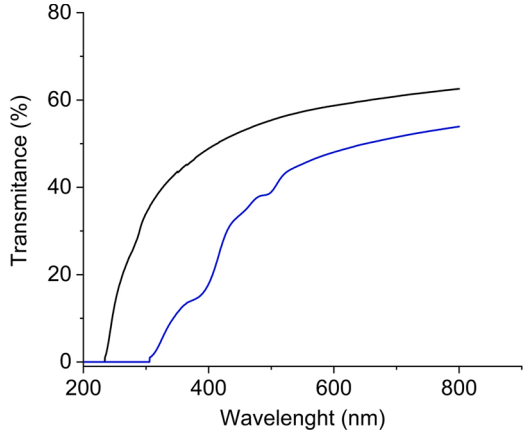

Fig. 5. UV-Vis light transmittance (%) of (—) CG and (——) CGPPE.

Table 3
Total phenolic content (TPC) and antioxidant activity against DPPH radical for PPE, CG and CGPPE; minimal inhibitory and bactericidal concentrations (MIC and MBC) against *S. aureus* and *S.* Enteritidis, for PPE, CG and CGPPE.

Parameters	PPE	CG	CGPPE
TPC (mg GAE g^{-1})	215.71 ± 5.95^{a}	0.015 ± 0.001^{c}	0.207 ± 0.020^{b}
IC	IC_{50}: 4.55 μg mL^{-1} [a]	–	IC_{20}: 38 mg mL^{-1} [b]
AAI	2.98	–	–
MIC *S. aureus* (μg mL^{-1})	125	31.2	31.2
MBC *S. aureus* (μg mL^{-1})	> 2000	31.2	31.2
MIC *S. Enteritidis* (μg mL^{-1})	500	125	125
MBC *S. Enteritidis* (μg mL^{-1})	> 2000	250	> 500

Different lowercase letters on the same line show statistically significant differences by ANOVA and Tukey ($p \leq 0.05$).

% inhibition versus log [PPE] was 4.55 μg mL^{-1} (Fig. S4). That IC_{50} value is equivalent to an AAI of 2.98, which is attributed to extracts with very strong antioxidant activity (Scherer & Godoy, 2009). Our results are similar to the ones reported by Pal et al. (2017) (IC_{50} of 16.78 μg mL^{-1}) and by Okonogi, Duangrat, Anuchpreeda, Tachakittirungrod, and Chowwanapoonpohn (2007) (IC_{50} of 3 μg mL^{-1}) for pomegranate extracts.

CGPPE film-forming solution presented an IC_{20} of 38 mg mL^{-1}; CG, in turn, was not able to inhibit the radical at any of the concentrations used (20 – 80 mg mL^{-1}). These results consolidate how the incorporation of active compounds from PPE imparted antioxidant potential for the developed materials, which without the extract would not be able to shield the polymeric matrix against oxidation, impairing the other properties of the films reported so far.

MIC and MBC of PPE, CG, and CGPPE solutions against *S. Enteritidis* (Gram-negative) and *S. aureus* (Gram-positive) were also evaluated (Table 3). PPE was able to inhibit both bacterial strains, however, no MBC was observed at the concentrations tested. Further, PPE was more effective against *S. aureus* compared to *S. Enteritidis*, probably due to the differences in the bacterial cell wall structure: the outer membrane in Gram-negative bacteria is less permeable to hydrophobic compounds, such as tannins and other flavonoids present in the extract (Celiksoy & Heard, 2021). It is also worth noting that the MIC values observed in our study for PPE were lower than the ones found in other studies for pomegranate extracts (Garcia et al., 2021; Rosas-Burgos et al., 2017).

CG solution exhibited remarkable bactericidal activity against both *S. aureus* and *S. Enteritidis*, showing better efficacy for Gram-positive bacteria. CGPPE had the same MIC and MBC values as CG for *S. aureus* but showed no bactericidal effect for *S. Enteritidis*. This may be caused by the crosslinking between the hydroxyl groups from PPE and the protonated amino groups of chitosan, which lowered the interaction of the polymer with the cell targets of *S. Enteritidis*, leading to no bactericidal effect, only bacteriostatic.

However, it is also worth remembering that in the optimization study (Section 3.1), the presence of PPE seems to have contributed to the increase in the halo of inhibition of the polymeric solutions against the fungus *Botrytis cinerea*, a result that more quantitatively reflects the effect of the extract, when compared to the results of MIC and MBC. Moreover, the strong antioxidant capacity of PPE can be advantageous to keep the performance of the developed packaging: considering that the mechanism involved in the antimicrobial activity is related to disruptions in the bacterial cell wall (Sudarshan, Hoover, & Knorr, 1992; Wu et al., 2019), PPE phenolic compounds can shield the oxidation of the polymeric network and make it able to interact for a longer time with cells, resulting in innovative strategies to control foodborne pathogens.

4. Conclusions

An optimized composition containing 0.8% chitosan, 0.2% gelatin and 1 mg g^{-1} PPE was chosen with the aid of chemometric tools, aiming the potential application as films for food packaging. The interactions of the phenolics compounds from PPE with the polymeric matrix were confirmed by spectroscopic and rheological analysis, and the effects of their incorporation led to improvements in water-related properties (as lower solubility and swelling), light barrier properties (transmittance reduced by 30%), and resistance of the films against deformation (as demonstrated in oscillatory rheological measurements) and elongation (5% higher for CGPPE). PPE, which presented a very strong antioxidant activity (AAI of 2.98), was also able to impart antioxidant activity to the film-forming solutions (CGPPE inhibited 20% of DPPH at 38 mg mL^{-1}). Moreover, antimicrobial results showed low inhibitory and bactericidal concentrations against Gram-positive and negative bacteria (31.2 – 500 μg mL^{-1}), both for PPE and for the film-forming solutions, due to the intrinsic antimicrobial activity of chitosan. All results pointed to positive effects of the addition of a by-product as an active compound for chitosan and gelatin packaging, being the effects of its incorporation evaluated and optimized in this system, in an unprecedented way, with the use of a central composite design.

CRediT authorship contribution statement

Mirella Romanelli Vicente Bertolo: Conceptualization, Data curation, Methodology, Writing – original draft, Writing – review & editing. **Lucas Danilo Dias**: Conceptualization, Methodology, Writing – original draft. **Josemar Gonçalves de Oliveira Filho**: Conceptualization, Methodology, Writing – original draft. **Fernanda Alves**: Methodology, Writing – original draft. **Crisiane Aparecida Marangon**: Methodology, Writing – original draft. **Virginia da Conceição Amaro Martins**: Conceptualization, Methodology, Writing – review & editing. **Marcos David Ferreira**: Writing – review & editing. **Vanderlei Salvador Bagnato**: Writing – review & editing. **Ana Maria de Guzzi Plepis**: Supervision, Writing – review & editing. **Stanislau Bogusz Junior**: Funding acquisition, Supervision, Writing – review & editing.

Declaration of Competing Interest

The authors declare that they have no known competing financial interests or personal relationships that could have appeared to influence the work reported in this paper. CGPPE formulation was applied at the Institute of Industrial Property (INPI), number BR 10 2021 026404 7.

Data availability

Data will be made available on request.

Acknowledgment

We gratefully thank Prof. Dr. Osvaldo Novais de Oliveira Junior (IFSC/USP) for granting us access to the CAM200 goniometer (KSV Instruments) and Dr. José Dirceu Vollet-Filho (IFSC/USP) for the Raman analysis.

Funding sources

This work was supported by the grants 2019/18748–8 (MRVB), 2019/13569–8 (LDD), 2018/24612–9 (JGOF), 2019/22799–7 and 2018/22214–6 (CAM), São Paulo Research Foundation (FAPESP). Moreover, the authors thank FAPESP (CEPOF 2013/07276–1) and INCT "Basic Optics and Applied to Life Sciences" (FAPESP 2014/50857–8, CNPq 465360/2014–9). The opinions, hypotheses and conclusions or recommendations expressed in this article are the responsibility of the author(s) and do not necessarily reflect the view of FAPESP.

Appendix A. Supporting information

Supplementary data associated with this article can be found in the online version at doi:10.1016/j.fpsl.2022.100986.

References

Abbastabar, B., Azizi, M. H., Adnani, A., & Abbasi, S. (2015). Determining and modeling rheological characteristics of quince seed gum. *Food Hydrocolloids, 43*, 259–264.
Akhtar, S., Ismail, T., Fraternale, D., & Sestili, P. (2015). Pomegranate peel and peel extracts: chemistry and food features. *Food Chemistry, 174*, 417–425.
Asdagh, A., et al. (2021). Production and characterization of nanocomposite film based on whey protein isolated/copper oxide nanoparticles containing coconut essential oil and paprika extract. *The Journal of Polymers and the Environment, 29*, 335–349.
ASTM. (2016). *Standard test methods for water vapor transmission of materials. Standard designations: E96/E96M-16. Annual book of ASTM standards.* Philadelphia, PA: American Society for Testing and Materials,.
ASTM. (2012). *StandarD Test Method for Tensile Properties of Thin Plastic Sheeting.* D882 – 12. ASTM International,.
Ay, Ç.Ö., Özcan, A. S., Erdoğan, Y., & Özcan, A. (2012). Characterization of Punica granatum L. peels and quantitatively determination of its biosorption behavior towards lead (II) ions and acid blue 40. *Colloids and Surfaces B, 100*, 197–204.
Azaza, Y. B., et al. (2022). Development and characterization of active packaging films based on chitosan and sardinella protein isolate: effects on the quality and the shelf life of shrimps. *Food Packaging and Shelf Life, 31*, Article 100796.
Bertolo, M. R. V., Leme, R., Martins, V. C. A., Plepis, A. M. G., & Bogusz Junior, S. (2021a). Rheological characterization of the influence of pomegranate peel extract addition and concentration in chitosan and gelatin coatings. *Polysaccharides, 2*(3), 648–660.
Bertolo, M. R. V., Martins, V. C. A., Horn, M. M., Brenelli, L. B., & Plepis, A. M. G. (2020). Rheological and antioxidant properties of chitosan/gelatin-based materials functionalized by pomegranate peel extract. *Carbohydrate Polymers, 228*, Article 115386.
Bertolo, M. R. V., Martins, V. C. A., Plepis, A. M. G., & Bogusz Junior, S. (2021b). Natural deep eutectic solvents as a green strategy to recover valuable phenolic compounds. *Journal of Cleaner Production, 327*, Article 129471.
Bertolo, M.R.V., Martins, V.C.A., Plepis, A.M.G., Bogusz Junior, S. (2021c). Polymeric compositions with antioxidant and antimicrobial properties for fruit coating, coating preparation method and its use. BR 10 2021 026404 7, applied at December 23rd, 2021.
Celiksoy, V., & Heard, C. M. (2021). *Antimicrobial Potential of Pomegranate Extracts* (1st ed., pp. 1–23). IntechOpen (Online).
Chen, T., et al. (2022). Biodegradable films of chitosan and tea polyphenols catalyzed by laccase and their physical and antioxidant activities. *Food Bioscience, 46*, Article 101513.
Chen, Z., Bertin, R., & Froldi, G. (2013). EC_{50} estimation of antioxidant activity in DPPH• assay using several statistical programs. *Food Chemistry, 138*, 414–420.
Clinical and Laboratory Standards Institute. (2018). Performance standards for antimicrobial susceptibility testing; 27th informational supplement. M100-S28. Clinical and Laboratory Standards Institute. *Wayne, Pennsylvania*.
Duan, C., et al. (2019). Chitosan as a preservative for fruits and vegetables: a review on chemistry and antimicrobial properties. *Journal of Bioresources and Bioproducts, 4*(1), 11–21.
Dutta, P. K., Tripathi, S., Mehrotra, G. K., & Dutta, J. (2009). Perspectives for chitosan based antimicrobial films in food applications. *Food Chemistry, 114*(4), 1173–1182.
Eddya, M., Tbib, B., & Hami, K. (2020). A comparison of chitosan properties after extraction from shrimp shells by diluted and concentrated acids. *Heliyon, 6*, Article e03486.
Edison, T. J. I., & Sethuraman, M. G. (2013). Biogenic robust synthesis of silver nanoparticles using Punica granatum peel and its application as a green catalyst for the reduction of an anthropogenic pollutant 4-nitrophenol. *Spectrochim Acta Part A, 104*, 262–264.
Fadavi, G., Mohammadifar, M. A., Zargarran, A., Mortazavian, A. M., & Komeili, R. (2014). Composition and physicochemical properties of Zedo gum exudates from *Amygdalus scoparia. Carbohydrate Polymers, 101*, 1074–1080.
Frushour, B. G., & Koenig, J. L. (1975). Raman scattering of collagen, gelatin, and elastin. *Biopolymers, 14*, 379–391.
Ganeson, K., et al. (2022). Improved functionality of cinnamon oil emulsion-based gelatin films as potential edible packaging film for wax apple. *Food Bioscience, 47*, Article 101638.
Garcia, C. F., et al. (2021). Development of collagen/nanohydroxyapatite scaffolds containing plant extract intended for bone regeneration. *Materials Science and Engineering C, 123*, Article 111955.
Horn, M. M., Martins, V. C. A., & Plepis, A. M. G. (2009). Interaction of anionic collagen with chitosan: effect on thermal and morphological characteristics. *Carbohydrate Polymers, 77*(2), 239–243.
Hu, H., Yao, X., Qin, Y., Yong, H., & Liu, J. (2020). Development of multifunctional food packaging by incorporating betalains from vegetable amaranth (*Amaranthus tricolor* L.) into quaternary ammonium chitosan/fish gelatin blend films. *International Journal of Biological Macromolecules, 159*, 675–684.
Hu, Z., & Gänzle, M. G. (2019). Challenges and opportunities related to the use of chitosan as a food preservative. *Journal of Applied Microbiology, 126*(5), 1318–1331.
Istiqomah, A., Utami, M. R., Firdaus, M., Suryanti, V., & Kusumaningsih, T. (2022). Antibacterial chitosan-Dioscorea alata starch film enriched with essential oils

optimally prepared by following response surface methodology. *Food Bioscience, 46*, Article 101603.
Jabraili, A., Pirsa, S., Pirouzifard, M. K., & Amiri, S. (2021). Biodegradable Nanocomposite Film Based on Gluten/Silica/Calcium Chloride: Physicochemical Properties and Bioactive Compounds Extraction Capacity. *Journal of Polymers and the Environment, 29*, 2557–2571.
Kaya, M., et al. (2018). Production and characterization of chitosan based edible films from Berberis crataegina's fruit extract and seed oil. *Innovative Food Science and Emerging Technologies, 45*, 287–297.
Konwar, A., Kalita, S., Kotoky, J., & Chowdhury, D. (2016). Chitosan–iron oxide coated graphene oxide nanocomposite hydrogel: a robust and soft antimicrobial biofilm. *ACS Applied Materials & Interfaces, 8*(32), 20625–20634.
Kumar, N. P. N., Petkoska, A. T., AL-Hilifi, S. A., & Fawole, O. A. (2021). Effect of chitosan–pullulan composite edible coating functionalized with pomegranate peel extract on the shelf life of mango (*Mangifera indica*). *Coatings, 11*, 764.
Kurita, K. (2006). Chitin and chitosan: functional biopolymers from marine crustaceans. *Marine Biotechnology, 8*(3), 203.
Lavertu, M., et al. (2003). A validated 1H NMR method for the determination of the degree of deacetylation of chitosan. *Journal of Pharmaceutical and Biomedical, 32*(6), 1149–1158.
Mandala, I. G., Savvas, T. P., & Kostaropoulos, A. E. (2004). Xanthan and locust bean gum influence on the rheology and structure of a white model-sauce. *Journal of Food Engineering, 64*, 335–342.
Mi, F. (2005). Synthesis and characterization of a novel chitosan−gelatin bioconjugate with fluorescence emission. *Biomacromolecules, 6*(2), 975–987.
Nair, S. B., Jyothi, A. N., Sajeev, M. S., & Misra, R. (2011). Rheological, mechanical and moisture sorption characteristics of cassava starch-konjac glucomannan blend films. *Starch, 63*(11), 728–739.
Naji-Tabasi, S., Mohammad, S., & Razavi, A. (2017). New studies on basil (*Ocimum bacilicum* L) seed gum: Part III steady and dynamic shear rheology. *Food Hydrocolloids, 67*, 243–250.
Narasagoudr, S. S., et al. (2020). Physico-chemical and functional properties of rutin induced chitosan/poly (vinyl alcohol) bioactive films for food packaging applications. *Food Hydrocolloids, 109*, Article 106096.
Okonogi, S., Duangrat, C., Anuchpreeda, S., Tachakittirungrod, S., & Chowwanapoonpohn, S. (2007). Comparison of antioxidant capacities and cytotoxicities of certain fruit peels. *Food Chemistry, 103*, 839–846.
Oliveira Filho, J. G., et al. (2019). Active food packaging: alginate films with cottonseed protein hydrolysates. *Food Hydrocolloids, 92*, 267–275.
Oliveira Filho, J. G., et al. (2020). New approach in the development of edible films: The use of carnauba wax micro-or nanoemulsions in arrowroot starch-based films. *Food Packaging and Shelf Life, 26*, Article 200589.
Pal, J., Raju, C. V., Pandey, G., Raj, R., & Singh, R. R. (2017). Antioxidant activity of pomegranate peel extract and its effect on storage stability of cooked meat model system of indian mackerel (*Rastrelliger kanagurta*) stored at 4 ± 2 °C. *Biochemical and Cellular Archives, 17*(1), 183–187.
Peng, Y., & Li, Y. (2014). Combined effects of two kinds of essential oils on physical, mechanical and structural properties of chitosan films. *Food Hydrocolloids, 36*, 287–293.
Peng, Y., Wu, Y., & Li, Y. (2013). Development of tea extracts and chitosan composite films for active packaging materials. *International Journal of Biological Macromolecules, 59*, 282–289.
Pirsa, S., Farshchi, E., & Roufegarinejad, L. (2020). Antioxidant/Antimicrobial Film Based on Carboxymethyl Cellulose/Gelatin/TiO2–Ag Nano-Composite. *Journal of Polymers and the Environment, 28*, 3154–3163.
Pirsa, S., Sani, I. K., Pirouzifard, M. K., & Erfani, A. (2020). Smart film based on chitosan/ *Melissa officinalis* essences/ pomegranate peel extract to detect cream cheeses spoilage. *Food Additives & Contaminants: Part A, 37*(4), 634–648.
Poverenov, E., et al. (2014). Effects of a composite chitosan–gelatin edible coating on postharvest quality and storability of red bell peppers. *Postharvest Biology and Technology, 96*, 106–109.
Qin, Y. Y., et al. (2015). Physio-mechanical properties of an active chitosan film incorporated with montmorillonite and natural antioxidants extracted from pomegranate rind. *Journal of Food Science and Technology, 52*, 1471–1479.
Rinaudo, M. (2006). Chitin and chitosan: Properties and applications. *Progress in Polymer Science, 31*, 603–632.
Rosas-Burgos, E. C., et al. (2017). Antimicrobial activity of pomegranate peel extracts as affected by cultivar. *Journal of the Science of Food and Agriculture, 97*, 802–810.
Roy, S., & Rhim, J. W. (2021). Fabrication of bioactive binary composite film based on gelatin/chitosan incorporated with cinnamon essential oil and rutin. *Colloids and Surfaces B, 204*, Article 111830.
Salem, M. N., Albanna, L. S., & Awwad, A. M. (2017). Nano-structured zinc sulfide to enhance *Cucumis sativus* (cucumber) plant growth. *American Journal of Agricultural and Biological Sciences, 12*(5), 167–173.
Scherer, R., & Godoy, H. T. (2009). Antioxidant activity index (AAI) by the 2,2-diphenyl-1-picrylhydrazyl method. *Food Science, 112*(13), 654–658.
Sharifi, K. A., & Pirsa, S. (2021). Biodegradable film of black mulberry pulp pectin/ chlorophyll of black mulberry leaf encapsulated with carboxymethylcellulose/silica nanoparticles: Investigation of physicochemical and antimicrobial properties. *Materials Chemistry and Physics, 267*, Article 124580.
Singleton, V. L., Orthofer, R., & Lamuela-Raventós, R. M. (1999). Analysis of total phenols and other oxidation substrates and antioxidants by means of Folin-Ciocalteu reagent. *Methods in Enzymology, 299*, 152–178.
Steffe, J. F. (1996). *Rheological Methods in Food Process Engineering*. East lansing, MI, USA: Freeman Press,.
Sudarshan, N. R., Hoover, D. G., & Knorr, D. (1992). Antibacterial action of chitosan. *Food Biotechnology, 6*, 257–272.
Tang, C., Guan, Y., Yao, S., & Zhu, Z. (2007). Preparation of ibuprofen-loaded chitosan films for oral mucosal drug delivery using supercritical solution impregnation. *International Journal of Pharmaceutics, 473*(1–2), 434–441.
Theapsak, S., Watthanaphanit, A., & Rujiravanit, R. (2012). Preparation of chitosan-coated polyethylene packaging films by DBD plasma treatment. *ACS Applied Materials & Interfaces, 4*(5), 2474–2482.
Wu, S. C., et al. (2019). Antibacterial effect and mode of action of flavonoids from licorice against methicillin-resistant *Staphylococcus aureus*. *Front Microbiology, 10*, 1–14.
Xu, X. H., Ren, G. L., Cheng, J., Liu, Q., Li, D. G., & Chen, Q. (2006). Self-assembly of polyaniline-grafted chitosan/glucose oxidase nanolayered films for electrochemical biosensor applications. *Journal of Materials Science, 41*(15), 4974–4977.
Xue, F., et al. (2021). Physicochemical properties of chitosan/zein/essential oil emulsion-based active films functionalized by polyphenols. *Future Foods, 3*, Article 100033.
Yu, D., Yu, Z., Zhao, W., Regenstein, J. M., & Xia, W. (2021). Advances in the application of chitosan as a sustainable bioactive material in food preservation. *Critical Reviews in Food Science and Nutrition*, 1–36.
Yuan, G., Lv, H., Yang, B., Chen, X., & Sun, H. (2015). Physical properties, antioxidant and antimicrobial activity of chitosan films containing carvacrol and pomegranate peel extract. *Molecules, 20*, 11034–11045.
Zeng, J., Ren, X., Zhu, S., & Gao, Y. (2021). Fabrication and characterization of an economical active packaging film based on chitosan incorporated with pomegranate peel. *International Journal of Biological Macromolecules, 192*, 1160–1168.